Supramolecular Chemistry
Publication details, including instructions for authors and subscription information:
http://www.informaworld.com/smpp/title~content=t713649759

Dimerisation and complexation of 6-(4'-*t*-butylphenylamino)naphthalene-2-sulphonate by β-cyclodextrin and linked β-cyclodextrin dimers

Duc-Truc Pham[a]; Philip Clements[a]; Christopher J. Easton[b]; John Papageorgiou[a]; Bruce L. May[a]; Stephen F. Lincoln[a]
[a] School of Chemistry and Physics, University of Adelaide, Adelaide, Australia [b] Research School of Chemistry, Australian National University, Canberra, Australia

To cite this Article Pham, Duc-Truc , Clements, Philip , Easton, Christopher J. , Papageorgiou, John , May, Bruce L. and Lincoln, Stephen F.(2009) 'Dimerisation and complexation of 6-(4'-*t*-butylphenylamino)naphthalene-2-sulphonate by β-cyclodextrin and linked β-cyclodextrin dimers', Supramolecular Chemistry, 21: 6, 510 — 519
To link to this Article: DOI: 10.1080/10610270802406579
URL: http://dx.doi.org/10.1080/10610270802406579

Supramolecular Chemistry
Vol. 21, No. 6, September 2009, 510–519

Taylor & Francis
Taylor & Francis Group

Dimerisation and complexation of 6-(4′-*t*-butylphenylamino)naphthalene-2-sulphonate by β-cyclodextrin and linked β-cyclodextrin dimers

Duc-Truc Pham[a], Philip Clements[a], Christopher J. Easton[b], John Papageorgiou[a], Bruce L. May[a] and Stephen F. Lincoln[a]*

[a]*School of Chemistry and Physics, University of Adelaide, Adelaide, Australia;* [b]*Research School of Chemistry, Australian National University, Canberra, Australia*

(*Received 23 April 2008; final version received 23 July 2008*)

This study shows that stereochemical factors largely determine the extent to which 6-(4′-*t*-butylphenylamino)-naphthalene-2-sulphonate, BNS^- and its dimer, $(BNS^-)_2$, are complexed by β-cyclodextrin, βCD, and a range of linked βCD dimers. Fluorescence and ^{1}H NMR studies, respectively, show that BNS^- and $(BNS^-)_2$ form host–guest complexes with βCD of the stoichiometry βCD.BNS^- ($10^{-4}K_1 = 4.67\,dm^3\,mol^{-1}$) and βCD.$BNS_2^{2-}$ ($10^{-2}K_2' = 2.31\,dm^3\,mol^{-1}$), where the complexation constant $K_1 = [\beta CD.BNS^-]/([\beta CD][BNS^-])$ and $K_2' = [\beta CD.(BNS^-)_2]/([\beta CD.BNS^-][BNS^-])$ in aqueous phosphate buffer at pH 7.0, $I = 0.10\,mol\,dm^3$ at 298.2 K. (The dimerisation of BNS^- is characterised by $10^{-2}K_d = 2.65\,dm^3\,mol^{-1}$.) For *N*,*N*-bis((2^{A}S,3^{A}S)-3^A-deoxy-3^A-β-cyclodextrin)succinamide, 33βCD$_2$su, *N*-((2^{A}S,3^{A}S)-3^A-deoxy-3^A-β-cyclodextrin)-*N*′-(6^A-deoxy-6^A-β-cyclodextrin)urea, 36βCD$_2$su, *N*,*N*-bis(6^A-deoxy-6^A-β-cyclodextrin)-succinamide, 66βCD$_2$su, *N*-((2^{A}S,3^{A}S)-3^A-deoxy-3^A-β-cyclodextrin)-*N*′-(6^A-deoxy-6^A-β-cyclodextrin)urea, 36βCD$_2$ur, and *N*,*N*-bis(6^A-deoxy-6^A-β-cyclodextrin)urea, 66βCD$_2$ur, the analogous $10^{-4}K_1 = 11.0$, 101, 330, 29.6 and 435 $dm^3\,mol^{-1}$ and $10^{-2}K_2' = 2.56$, 2.31, 2.59, 1.82 and 1.72 $dm^3\,mol^{-1}$, respectively. A similar variation occurs in K_1 derived by UV–vis methods. The factors causing the variations in K_1 and K_2 are discussed in conjunction with ^{1}H ROESY NMR and molecular modelling studies.

Keywords: cyclodextrin; fluorescence; host–guest; NMR spectroscopy; supramolecular

Introduction

The modification of cyclodextrins (CDs) has introduced increasing sophistication into host–guest complexation studies wherein a CD host complexes a guest species (*1*). Among such modified CDs are linked CD-dimers (*2–7*) in which the linker may be substituted onto the CD at either the C2^A, C3^A or C6^A carbon of a glucopyranose unit. Such variations in substitution and the nature of the linker can significantly influence guest complexation (*8–14*). The effects of these factors are explored herein through complexation of the guest 6-(4′-*t*-butylphenyl-amino)-naphthalene-2-sulphonate, BNS^- (Figure 1). The BNS^- monomer and $(BNS^-)_2$ dimer are in equilibrium in aqueous solution and both are complexed by β-cyclodextrin, βCD and linked βCD-dimers. Thus, an opportunity arises to quantify multiple equilibria that are much less well characterised in host–guest chemistry.

β-Cyclodextrin, the α-1,4-joined heptamer of glucopyranose in which the 7 primary and 14 secondary hydroxyl groups, respectively, delineate the narrow and wider ends of an annulus whose hydrophobic interior is lined with methine and methylene hydrogens and ether oxygens, and five linked βCD-dimers are chosen as hosts in this study (Figure 1). The linkers of the βCD-dimers are substituted onto either a C3 (with inversion) or a C6 of βCD. These dimers are *N*,*N*-bis((2^{A}S,3^{A}S)-3^A-deoxy-3^A-β-cyclodextrin)succinamide, 33βCD$_2$su, *N*-((2^{A}S,3^{A}S)-3^A-deoxy-3^A-β-cyclodextrin)-*N*′-(6^A-deoxy-6^A-β-cyclodextrin)urea, 36βCD$_2$su, *N*,*N*-bis(6^A-deoxy-6^A-β-cyclodextrin)succinamide, 66βCD$_2$su, *N*-((2^{A}S,3^{A}S)-3^A-deoxy-3^A-β-cyclodextrin)-*N*′-(6^A-deoxy-6^A-β-cyclodextrin)urea, 36βCD$_2$ur, and *N*,*N*-bis(6^A-deoxy-6^A-β-cyclodextrin) urea, 66βCD$_2$ur (Figure 1; *7, 15*). (The preparation of *N*,*N*-bis((2^{A}S,3^{A}S)-3^A-deoxy-3^A-β-cyclodextrin)urea, 33βCD$_2$ur, to complete the series failed evidently because of steric hindrance (*15*).) The altrose inversion about C3 in the linking glucopyranose unit constricts the βCD annulus and provides an opportunity to systematically study the effect of such constriction on cooperativity in the complexation of BNS^- by linked βCD dimers.

Results and discussion

UV–vis and ^{1}H NMR studies of dimerisation of BNS^-

Over the concentration range 5.06×10^{-6}–$4.93 \times 10^{-5}\,mol\,dm^{-3}$ BNS^- exhibits a linear increase in UV–vis absorbance in the range 220–360 nm in aqueous phosphate buffer (pH 7.0, $I = 0.10\,mol\,dm^{-3}$, 298.2 K)

*Corresponding author. Email: stephen.lincoln@adelaide.edu.au

ISSN 1061-0278 print/ISSN 1029-0478 online

DOI: 10.1080/10610270802406579
http://www.informaworld.com

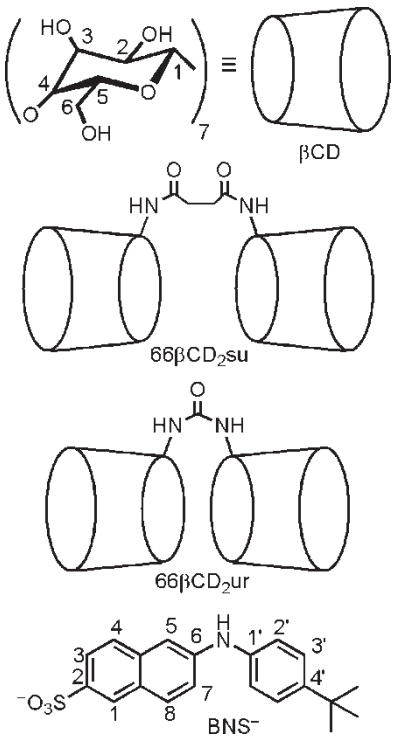

Figure 1. Structures of β-cyclodextrin species and BNS^-. In $66\beta CD_2ur$ and $66\beta CD_2ur$ both βCD are linked through $C6^A$, in $36\beta CD_2ur$ and $36\beta CD_2ur$ one βCD is linked through $C3^A$ and the other through $C6^A$, and in $33\beta CD_2su$ both βCD are linked through $C3^A$.

consistent with no significant formation of the $(BNS^-)_2$ dimer. However, over the higher concentration range $0.02–4.00 \times 10^{-2}$ mol dm^{-3}, BNS^- the ^{1}H NMR resonance of the *t*-butyl group moves upfield with increasing $[BNS^-]_{total}$ consistent with increasing shielding as shown

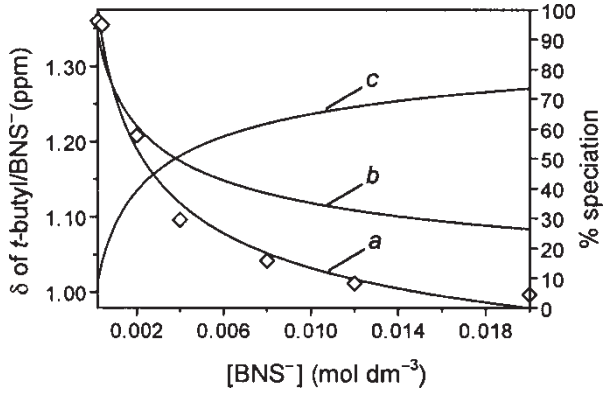

Figure 2. Left ordinate: variation of the ^{1}H (300 MHz) chemical shift of the *t*-butyl resonance of BNS^- with $[BNS^-]_{total}$ (0.02, 0.04, 0.02, 0.04, 0.08, 0.12 and 0.20×10^{-2} mol dm^{-3}), where curve *a* is the best fit of the algorithm for dimerisation of BNS^- to the chemical shift variation. Right ordinate: speciation with $[BNS^-]_{total} \equiv 100\%$, curve *b* = BNS^- % and curve *c* = BNS^- % existing as $(BNS^-)_2$.

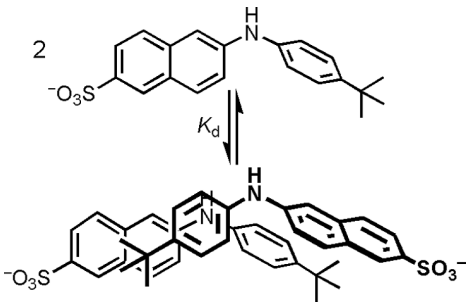

Figure 3. Dimerisation of BNS^-.

in Figure 2. (All NMR studies were carried out in D_2O phosphate buffer solution at *p*D 7.0, $I = 0.10$ mol dm^{-3}, 298.2 K.) This indicates the formation of a $(BNS^-)_2$ dimer in which the *t*-butyl protons of one BNS^- experience shielding as a consequence of being in close proximity to the high π electron density of the naphthyl group of a second BNS^- in a dimer structure approximating to that shown in Figure 3. The naphthyl and phenyl planes are represented as mutually 60° to each other as MM2 (Chem3D) gas phase modelling indicates (*16*). A ^{1}H ROESY NMR spectrum of a $[BNS^-]_{total} = 2.0 \times 10^{-2}$ mol dm^{-3} D_2O solution showed cross-peaks between the *t*-butyl protons and the 1, 3 and 4 protons of BNS^- (Figure 4) consistent with this dimer structure. (The *t*-butyl protons are >400 pm distant from the 5, 6 and 7 protons within a single BNS^- anion such that through-space dipolar interactions should be too weak to produce significant ROESY cross-peaks.) Fitting of an algorithm for BNS^- dimerisation to the variation of δ for *t*-butyl with concentration (Figure 2) yields a dimerisation constant, $K_d = 265 \pm 5$ dm^3 mol^{-1}. This small K_d is consistent with insignificant formation of $(BNS^-)_2$ under the more dilute conditions of the UV–vis and fluorescence studies described below.

The related 6-(4′-methylphenylamino)naphthalene-2-sulphonate, TNS^-, which has a methyl group in the same position as the *t*-butyl group in BNS^-, does not show significant changes in δ over the same concentration range as does BNS^-. This suggests that either the δ of TNS^- is less sensitive to dimerisation than is the δ of BNS^-, or K_d for $(TNS^-)_2$ is significantly less than that for $(BNS^-)_2$. If the latter is the case, this may be because of the smaller size of the methyl group, by comparison with a *t*-butyl group, causing the overall hydrophobicity of TNS^- to be less than that of BNS^- and a lesser tendency to dimerise. These factors also appear to cause differentiation between TNS^- and BNS^- complexation by βCD and the linked βCD-dimers as is discussed below. (Structure and charge cause significant variations in K_d as exemplified by tropaeolin 000 no. 2 anion (910 dm^3 mol^{-1}), crystal violet cation (600 dm^3 mol^{-1}), roccellin anion (1640 dm^3 mol^{-1}) and pyronine B cation (1300 dm^3 mol^{-1}; *17*)).

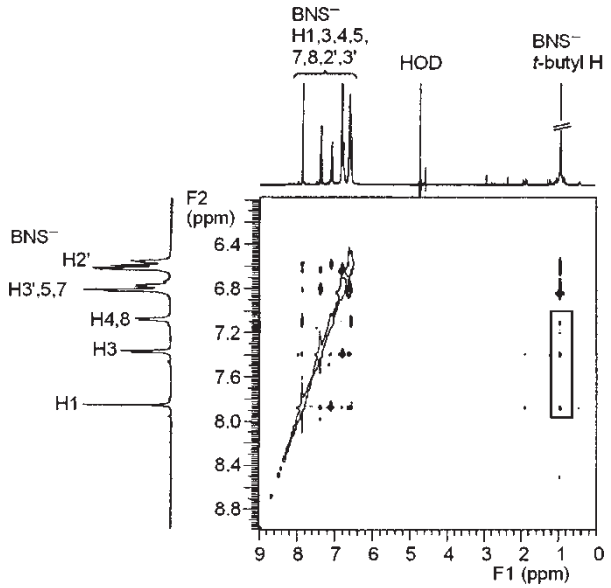

Figure 4. ^{1}H ROESY NMR spectrum of a $[BNS^-]_{total} = 2.0 \times 10^{-2}$ mol dm^{-3} solution. Cross-peaks arising from the interaction of the *t*-butyl and 1, 3 and 4 protons of BNS^- are enclosed in the rectangle. For $K_d = 265$ dm^3 mol^{-1}, 7.35×10^{-3} mol dm^{-3} of BNS^- exists as $(BNS^-)_2$.

UV–vis complexation studies

The UV–vis variation of the spectrum of BNS^- ($\lambda_{max} = 265.0$ and 317.0 nm, $\varepsilon = 22{,}000$ and 17,500 dm^3 mol^{-1} cm^{-1}) with increasing $[\beta CD]_{total}$ as formation of $\beta CD.BNS^-$ ($\lambda_{max} = 267.0$ and 317.5 nm, $\varepsilon = 24{,}500$ and 19,400 dm^3 mol^{-1} cm^{-1}) occurs is shown in Figure 5. The best fit of an algorithm for the formation of the 1:1 host–guest complex, $\beta CD.BNS^-$, to this UV–vis variation appears in Figure 6. Similar UV–vis variations of the BNS^- spectrum are observed in the presence of the linked

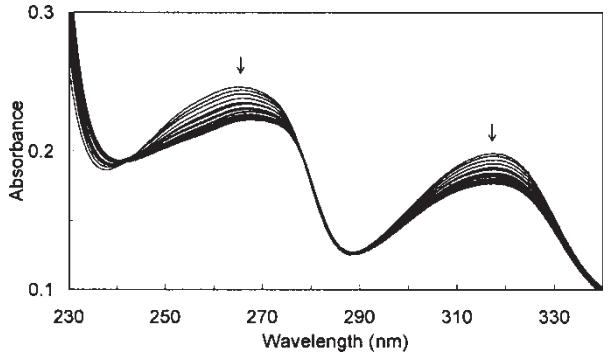

Figure 5. UV–vis absorption changes at 298.2 K shown by BNS^- (1.00×10^{-5} mol dm^{-3}) with $[\beta CD]_{total}$ in the range 0, 4.00 and 8.00×1.0^{-6}, 1.21, 1.60, 2.00, 2.39, 2.78, 3.18, 3.57, 3.99, 4.45, 5.04, 5.40, 6.42, 7.16, 8.38 and 9.54×10^{-5}, 1.11, 1.28, 1.44, 1.59, 1.79 and 1.99×10^{-4} mol dm^{-3}. The arrows indicate the direction of absorbance change as $[\beta CD]_{total}$ increases. An isosbestic point occurs at 241.0 nm.

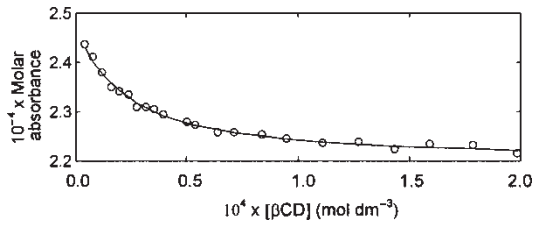

Figure 6. Absorbance variation of BNS^- with $[\beta CD]_{total}$ at 265 nm under the same conditions as in Figure 5. The solid curve represents the best fit obtained over the ranges 245–275 nm and 300–335 nm at 0.25 nm intervals.

βCD-dimers $66\beta CD_2su$ and $36\beta CD_2su$ (Figures 7 and 8, respectively). The only host–guest complexes detected are 1:1 species, as exemplified by $66\beta CD_2su.BNS^-$ in Figure 9, consistent with the appearance of several

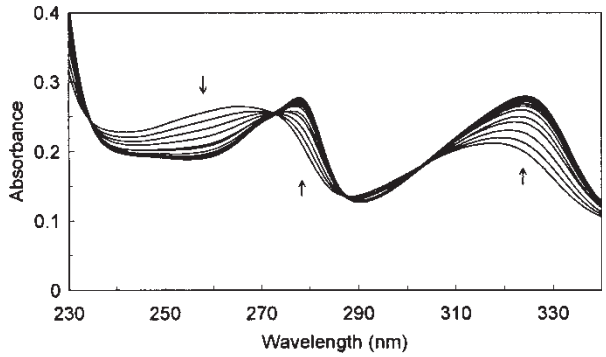

Figure 7. UV–vis absorption changes at 298.2 K shown by BNS^- (1.00×10^{-5} mol dm^{-3}) with $[66\beta CD_2su]_{total}$ in the range 0, 1.96, 4.02, 6.12 and 8.10×1.0^{-6}, 1.01, 1.20, 1.40, 1.60, 1.79, 1.99, 2.23, 2.48, 2.74, 3.17, 3.62, 4.24, 4.85, 5.65, 6.47, 7.27, 8.09, 9.11 and 9.99×10^{-5} mol dm^{-3}. The arrows indicate the direction of absorbance change as $[66\beta CD_2su]_{total}$ increases. Isosbestic points occur at 235.0, 272.5, 287.5 and 302.0 nm.

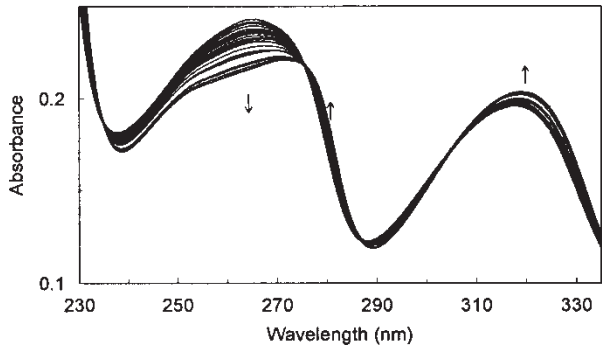

Figure 8. UV–vis absorption changes at 298.2 K shown by BNS^- (1.00×10^{-5} mol dm^{-3}) with $[36\beta CD_2su]_{total}$ in the range 0, 4.00 and 8.00×1.0^{-7},1.20, 1.59, 2.00, 2.38, 2.78. 3.17, 3.57, 3.96, 4.47, 4.97, 5.58, 6.39, 7.15, 8.28 and 9.57×1.0^{-6}, 1.11, 1.26, 1.43, 1.57, 1.78 and 1.97×10^{-5} mol dm^{-3}. The arrows indicate the direction of absorbance change as $[36\beta CD_2su]_{total}$ increases. Isosbestic points occur at 235.0, 275.0, 286.5 and 306.0 nm.

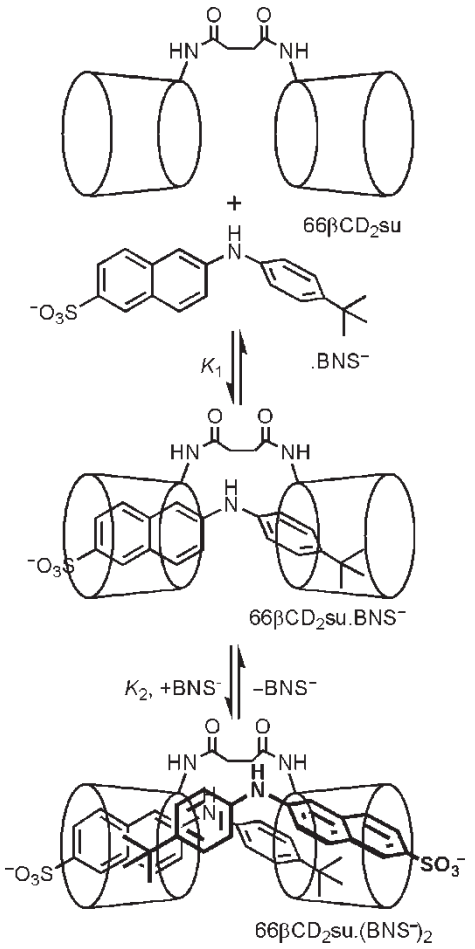

Figure 9. Complexation equilibria.

isosbestic points. The derived K_1 appears in Table 1. (All UV–vis studies refer to aqueous phosphate buffer solutions at p H 7.0, $I = 0.10\,\text{mol dm}^{-3}$ and 298.2 K.)

While the change induced in the spectrum of BNS^- by 66βCD$_2$su ($\lambda_{max} = 278.0$ and 325 nm, $\varepsilon = 28{,}000$ and 28,500 dm^3 mol^{-1} cm^{-1}) differs markedly from that induced by βCD, this difference is less for 36βCD$_2$su ($\lambda_{max} = 273.0$ and 318.0 nm, $\varepsilon = 22{,}100$ and 19,700 dm^3 mol^{-1} cm^{-1}) and 33βCD$_2$su ($\lambda_{max} = 270.0$ and 320.0 nm, $\varepsilon = 22{,}900$ and 18,800 dm^3 mol^{-1} cm^{-1}). A similar relationship holds for 66βCD$_2$ur ($\lambda_{max} = 278.0$ and 324.0 nm, $\varepsilon = 24{,}600$ and 25,100 dm^3 mol^{-1} cm^{-1}) and 36βCD$_2$ur ($\lambda_{max} = 267.0$ and 318.0 nm, $\varepsilon = 22{,}200$ and 17,400 dm^3 mol^{-1} cm^{-1}). The equivalent C6^A substituted βCD of 66βCD$_2$su and 66βCD$_2$ur limit the orientations of the ends of BNS^- simultaneously complexed in both annuli to a single orientation with respect to the primary and secondary ends of the annuli. However, BNS^- complexing in 33βCD$_2$su reverses this orientation, whereas complexing in 36βCD$_2$su and 36βCD$_2$ur potentially offers a choice of orientation.

As the spectra of 66βCD$_2$su.BNS^- and 66βCD$_2$ur.BNS^- differ most from that of βCD.BNS^-, it may be inferred that the dominant orientation of BNS^- in the latter complex has the *t*-butyl group adjacent to the primary hydroxy end of the βCD annulus as is necessarily the case in 33βCD$_2$su.BNS^-. While BNS^- has the choice of two opposite orientations when complexed in the C3^A and C6^A substituted βCD of 36βCD$_2$su.BNS^- and 36βCD$_2$ur.BNS^- that with the *t*-butylphenyl group is probably favoured as indicated by the similarity of the UV–vis spectra of these complexes and that of βCD.BNS^-. (The complexation of the *t*-butylphenyl group of BNS^- by βCD and the simultaneous complexation of both ends of BNS^- by the linked βCD-dimers is supported by the ^{1}H ROESY NMR data discussed below.) Generally the changes in the absorbance spectrum of complexed BNS^- reflect changes in its hydration in the complexed environment and possibly some change in the angles between the planes of the phenyl and naphthyl entities

Table 1. Complexation constants for 1:1 host–guest complexes, K_1, determined by UV–vis and fluorescence spectroscopy, and for 1:2 host–guest complexes, K_2, determined from ^{1}H NMR spectroscopic data in aqueous phosphate buffer (*p*H 7.0 or *p*D 7.0, $I = 0.10\,\text{mol dm}^{-3}$) at 298.2 K.

Host	UV–vis $10^{-4}K_1$[a–c] dm^3 mol^{-1}	Fluorescence $10^{-4}K_1$[a–c] dm^3 mol^{-1}	^{1}H NMR $10^{-7}K_2$[a,c,d] dm^6 mol^{-2}	Calculated $10^{-2}K_2'$ dm^3 mol^{-1}	Fluorescence $10^{-4}K_1$[e] dm^3 mol^{-1}
	Guest = BNS^-	Guest = BNS^-	Guest = BNS^-	Guest = BNS^-	Guest = TNS^-
βCD	5.54 ± 0.02	4.67 ± 0.01	1.08 ± 0.03	2.31	0.33
33βCD$_2$su	18.6 ± 0.1	11.0 ± 0.1	2.82 ± 0.05	2.56	0.96
36βCD$_2$su	74.0 ± 0.6	101 ± 1	23.3 ± 0.4	2.31	0.87
66βCD$_2$su	125 ± 1	330 ± 1	85.4 ± 0.6	2.59	1.25
36βCD$_2$ur	16.1 ± 0.1	29.6 ± 1	5.4 ± 0.1	1.82	0.98
66βCD$_2$ur	364 ± 3	435 ± 2	74.9 ± 0.8	1.72	3.80

[a] The errors shown are those obtained from data fitting. When experimental error is taken into account, the overall error is ±3%.
[b] In water.
[c] The $10^{-4}K_1$ derived from the ^{1}H NMR data are, 3.4 ± 0.4, 12 ± 7, 83 ± 10, 147 ± 12, 13 ± 8 and 276 ± 140 dm^3 mol^{-1} in the host sequence listed above, respectively, and the corresponding $10^{-7}K_2$ are, 0.76 ± 0.50, 3.0 ± 0.7, 20 ± 1, 42 ± 12, 2.3 ± 0.6 and 48 ± 14, respectively.
[d] In D_2O.
[e] Ref. (*15*).

due to twisting about the —NH— group to optimise complexation in the linked βCD-dimers.

Fluorimetric complexation studies

The fluorescence increases shown by BNS^- on complexation by βCD and $66\beta CD_2su$ are substantial (Figures 10 and 11) consistent with decreased quenching by water dipoles through BNS^- complexation in the βCD and linked βCD annuli. The best fit of an algorithm for the formation of the 1:1 host–guest complex $66\beta CD_2su.BNS^-$ to this relative fluorescence variation appears in Figure 12.

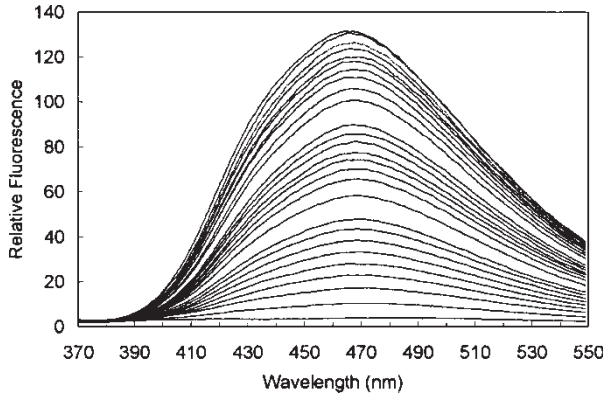

Figure 10. Increase in the relative fluorescence of BNS^- (1.00×10^{-6} mol dm^{-3}) with $[\beta CD]_{total}$ in the range 0, 1.00, 1.98, 2.96, 3.94, 4.96, 6.22, 7.40, 8.60 and 9.96×10^{-6}, 1.16, 1.32, 1.48, 1.64, 1.82, 2.00, 2.24, 2.48, 2.75, 3.16, 3.60, 4.20, 4.82, 5.41, 6.01, 6.62, 7.21, 8.04, 9.00 and 9.99×10^{-5} mol dm^{-3}. The excitation wavelength was 320 nm and the excitation and emission slit widths were 2.5 and 5 nm, respectively.

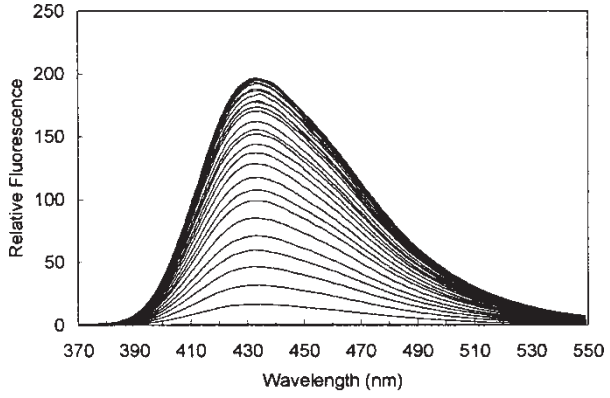

Figure 11. Increase in the relative fluorescence of BNS^- (1.00×10^{-6} mol dm^{-3}) with $[66\beta CD_2su]_{total}$ in the range 0, 1.02, 2.02, 3.00, 3.96, 4.94, 6.20, 7.46 and 8.66×10^{-7} and 1.00, 1.16, 1.32, 1.47, 1.64, 1.81, 2.03, 2.26, 2.49, 2.76, 3.15, 3.60, 4.23, 4.81, 5.40, 6.04, 6.61, 7.20, 8.03, 9.01 and 9.95×10^{-6} mol dm^{-3}. The excitation wavelength was 320 nm and the excitation and emission slit widths were 2.5 and 5 nm, respectively.

The corresponding K_1 derived for this system and the similarly derived K_1 of the other five systems appear in Table 1.

The BNS^- fluorescence maxima occur at 359 and 481.5 nm with relative fluorescences of 1.1 and 0.5 a.u. (arbitrary fluorescence units), respectively, while those for $\beta CD.BNS^-$ are 464.5 nm and 134 a.u. Substantially greater changes are observed for $66\beta CD_2su.BNS^-$ (433.0 nm, 209 a.u.), $36\beta CD_2su.BNS^-$ (432.0 nm, 154 a.u.), $33\beta CD_2su.BNS^-$ (436.5 nm, 137 a.u.), $66\beta CD_2ur.BNS^-$ (431 nm, 245 a.u.) and $63\beta CD_2su.BNS^-$ (436.5 nm, 142 a.u.). These changes are consistent with complexation in the hydrophobic βCD annulus changing the BNS^-environment and enhancing fluorescence as a consequence. (All fluorescence studies refer to aqueous phosphate buffer solutions at pH 7.0, $I = 0.10$ mol dm^{-3}, and 298.2 K.)

By analogy to closely related TNS^-, the changes in the observed λ_{max} are consistent with the existence of three excited states of BNS^- whose relative populations are environment dependent (*18*). Excitation ($\pi \rightarrow *\pi$) from the BNS^- S_0 ground state in which the planes of the naphthyl and phenyl groups are rotated 60° with respect to each other results in three BNS^- excited states. The first is $S_{1,np}$ (excitation $\lambda_{max} = 320$ nm, emission $\lambda_{max} = 482$ nm) in which the non-planarity is retained. Electron transfer produces two BNS^- charge transfer excited states: $S_{1-ct,np}$ (excitation $\lambda_{max} = 320–330$ nm, emission $\lambda_{max} \sim 400$ nm), where the naphthyl and phenyl planes approach co-planarity, and $S_{1-ct,perp}$ (excitation $\lambda_{max} = 290$ nm, emission $\lambda_{max} = 406$ nm) in which the naphthyl and phenyl planes are perpendicular to each other. In water the $S_{1-ct,perp}$ excited state dominates as a result of water hydrogen bonding to the amine nitrogen of BNS^- while the $S_{1-ct,np}$ and $S_{1,np}$ states are even less populated (Figure 13). However, in non-polar and viscous solvents, $S_{1,np}$ is expected to be dominantly populated. The latter solvent conditions resemble the hydrophobic and motion-restricting environment which BNS^- experiences in the βCD annulus (Figure 14). Accordingly, the decrease of the observed emission λ_{max} for BNS^- in the linked βCD-dimer complexes is consistent with $S_{1,np}$ becoming the dominant

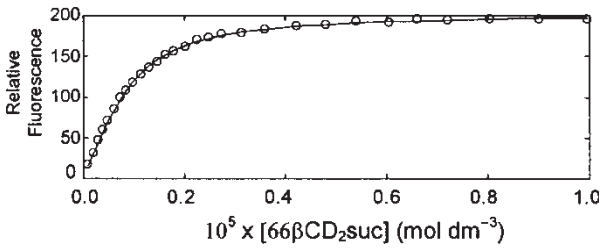

Figure 12. Relative fluorescence increase of BNS^- with $[66\beta CD_2su]_{total}$ at 433 nm under the same conditions as in Figure 11. The solid curve represents the best fit obtained over the range 400–500 nm at 0.5 nm intervals.

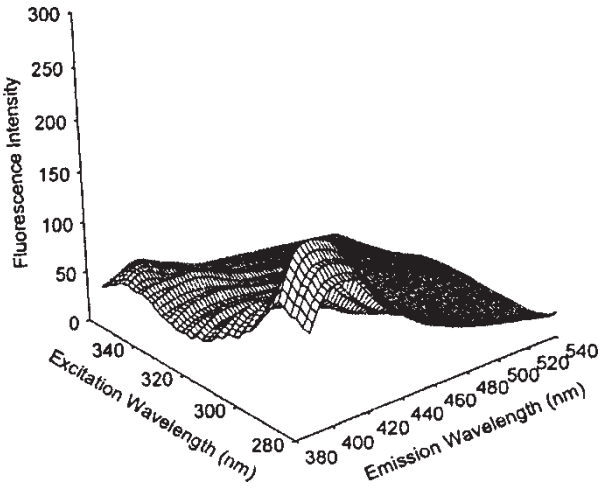

Figure 13. Three-dimensional plot of the fluorescence of BNS^- (1.0×10^{-5} mol dm^{-3}) as a function of excitation and emission wavelength at 2 nm intervals.

excited state as shown for $66\beta CD_2ur.BNS^-$, whereas the observed $\lambda_{max} = 406$ nm for BNS^- in water is a consequence of emission from the dominant $S_{1-ct,perp}$ excited state.

The increased BNS^- fluorescence with complexation probably results from a combination of three factors. The first is the decrease in the relative populations of the charge transfer $S_{1-ct,np}$ and $S_{1-ct,perp}$ excited states, which are likely to decay more rapidly than the $S_{1,np}$ excited state. The second is the isolation of BNS^- from the quenching pathway provided by water oscillators, and the third is the decrease in the number of rotational degrees of freedom for BNS^-, which also decreases the effectiveness of quenching (*19*).

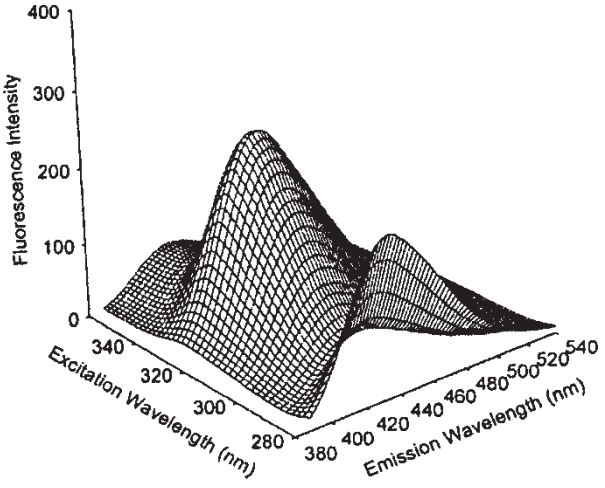

Figure 14. Three-dimensional plot of the fluorescence of BNS^- (1.0×10^{-6} mol dm^{-3}) and $66\beta CD_2ur.BNS^-$ (5.0×10^{-6} mol dm^{-3}) as a function of excitation and emission wavelength at 2 nm intervals. Under these conditions $[66\beta CD_2ur.BNS^-] = 0.95 \times 10^{-6}$ mol dm^{-3}.

1D and 2D ^{1}H ROESY NMR complexation studies

The 1D ^{1}H NMR studies were carried out at $[BNS^-]_{total}$ 50- and 500-fold greater than the UV–vis and fluorimetric studies. Consequently, formation of the $(BNS^-)_2$ dimer occurred simultaneously with BNS^- complexation by βCD and the linked βCD-dimers. The variation of δ for the *t*-butyl group of BNS^- with $[\beta CD]_{total}$ is shown in Figure 15 (where δ is equal to the sum of the mole fraction of BNS^- in each environment multiplied by its specific chemical shift). An algorithm incorporating $(BNS^-)_2$ and $\beta CD.BNS^-$ only could not be fitted to the variation of δ either when the K_d value determined by ^{1}H NMR spectroscopy was used as a constant, or when both the K_d value and the K_1 value determined fluorometrically were used as constants in the fitting procedure. However, incorporation of the formation of $\beta CD.(BNS^-)_2$($K_2 = [\beta CD.(BNS^-)_2]/\{[\beta CD][BNS^-]^2\}$) provided an excellent fit when K_1 and K_d were used as fixed values (Figure 15, which also shows the speciation of the system). When K_d alone was used as a fixed value, the K_1 and K_2 obtained were similar to those mentioned above, but the error was greater. Because the fluorimetrically determined K_1 and ^{1}H NMR-determined K_d were independently derived in the absence of spectral variations due to competing equilibria, their use as fixed values in the derivation of K_2 is likely to give the most reliable determination.

The increasing downfield shift of δ for the *t*-butyl group is broadly a consequence of the complexation of BNS^- in $\beta CD.BNS^-$ and $\beta CD.(BNS^-)_2$ inducing a downfield shift approximately twice the upfield shift caused by the dimerisation of BNS^-. The analogous data

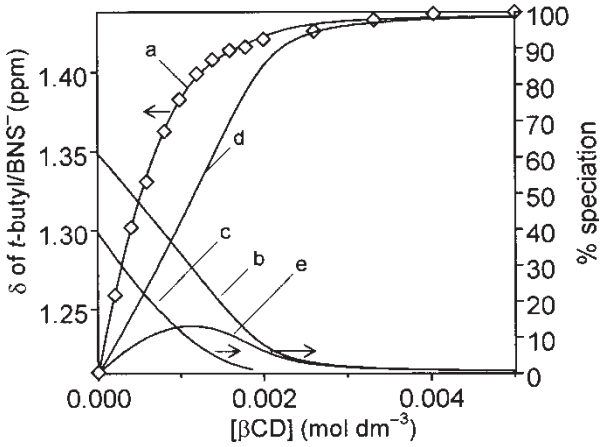

Figure 15. Left ordinate: variation of the ^{1}H (300 MHz) chemical shift of the *t*-butyl resonance of 2.00×10^{-3} mol dm^{-3} BNS^- with $[\beta CD]_{total}$ (0, 1.99, 3.98, 5.88, 8.05 and 9.86×10^{-4} and 1.19, 1.38, 1.59, 1.78, 2.00, 2.61, 3.32, 4.04 and 5.00×10^{-3} mol dm^{-3}) in D_2O, where curve *a* is the best fit of the algorithm for dimerisation of BNS^- to the chemical shift variation. Right ordinate: speciation with $[BNS^-]_{total} \equiv 100\%$, curves $b = BNS^-$ %, $c = BNS^-$ % existing as $(BNS^-)_2$, $d = \beta CD.BNS^-$ % and $e = BNS^-$ % existing as $\beta CD.(BNS^-)_2$%.

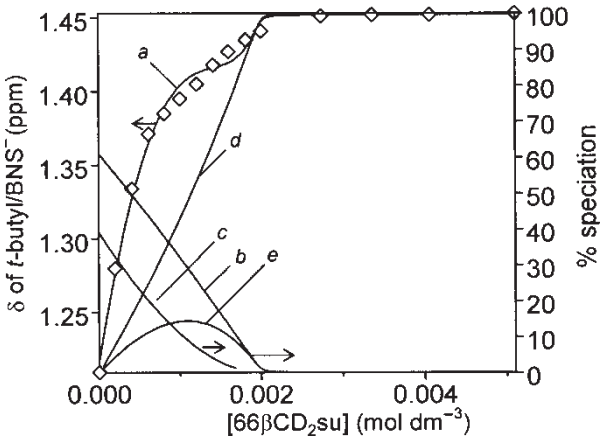

Figure 16. Left ordinate: variation of the ^{1}H (300 MHz) chemical shift of the *t*-butyl resonance of 2.00×10^{-3} mol dm^{-3} BNS^- with $[66\beta CD_2su]_{total}$ (0, 1.95, 4.09, 6.14 and 8.09×10^{-4} and 1.00, 1.21, 1.41, 1.60, 1.81, 2.00, 2.73, 3.36, 4.06 and 5.10×10^{-3} mol dm^{-3}) in D_2O, where curve *a* is the best fit of the algorithm for dimerisation of BNS^- to the chemical shift variation. Right ordinate: speciation with $[BNS^-]_{total} \equiv 100\%$, curves $b = BNS^-\%$, $c = BNS^-\%$ existing as $(BNS^-)_2$, $d = 66\beta CD_2su.BNS^-$ % and $e = BNS^-$ % existing as $66\beta CD_2su.(BNS^-)_2$%.

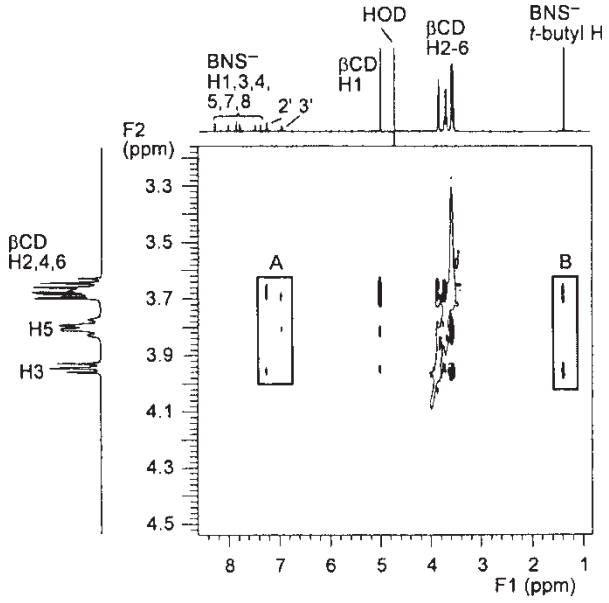

Figure 17. 2D ^{1}H ROESY NMR (600 MHz) spectrum of a D_2O solution equimolar at 2.00×10^{-3} mol dm^{-3} in BNS^- and βCD. The rectangles drawn on the spectrum, A and B, contain the cross-peaks arising from the NOE interactions between the annular H1, H3 and H5 protons of βCD and the aromatic protons of BNS^- and the *t*-butyl protons of BNS^-, respectively.

appear in Figure 16 for the $66\beta CD_2su.BNS^-/66\beta CD_2su.(BNS^-)_2$ system formed through the equilibria shown in Figure 9. The derived K_2 values for all six systems appear in Table 1.

2D ^{1}H ROESY NMR studies of complexation of BNS^- were carried out at equimolar 2.00×10^{-3} mol dm^{-3} concentrations of BNS^- and either βCD or one of the linked βCD-dimers, under which conditions the 1:1 host–guest complex is the greatly dominant species in solution as is seen from the speciation plots in Figures 15 and 16. The cross-peaks arising from dipolar interactions between BNS^- and βCD protons in $\beta CD.BNS^-$ arise dominantly from interactions between the 2′, 3′ and *t*-butyl BNS^- protons and those of βCD H3, H5 and H6 (although H6 cannot be clearly distinguished from H2 and H4) (*20*) with the naphthyl protons generating no cross-peaks (Figure 17). This is consistent with the hydrophobic *t*-butyl-phenyl group occupying the βCD annulus, whilst the more polar naphthalene-2-sulphonate group resides outside the βCD annulus. In contrast, most of the BNS^- protons form cross-peaks with those of $66\beta CD_2su$ consistent with simultaneous complexation of BNS^- in the linked βCD annuli of $66\beta CD_2su.BNS^-$ (Figure 18). (The $66\beta CD_2su$ proton resonances consist of a broad range of overlapping multiplets because substitution at $C6^A$ renders the seven glucopyranose units inequivalent as is also the case for substitution at $C3^A$.) The spectra of $36\beta CD_2su.BNS^-$, $33\beta CD_2su.BNS^-$, $36\beta CD_2ur.BNS^-$ and $66\beta CD_2ur.BNS^-$ also show cross-peaks arising from most of the BNS^- protons, but some of the aromatic resonances of the first

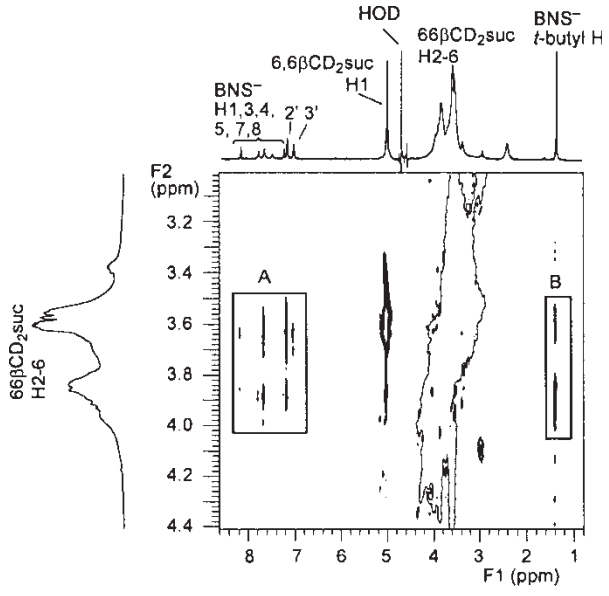

Figure 18. 2D ^{1}H ROESY NMR (600 MHz) spectrum of a D_2O solution equimolar at 2.00×10^{-3} mol dm^{-3} in BNS^- and $66\beta CD_2su$. The rectangles drawn on the spectrum, A and B, contain the cross-peaks arising from the NOE interactions between the annular H1, H3 and H5 protons of βCD and the aromatic protons of BNS^- and the *t*-butyl protons of BNS^-, respectively.

three complexes are substantially broadened in contrast to the *t*-butyl resonance, which shows little broadening. This suggests some restraint on rotation of the BNS^- guest within the host βCD annuli. Despite this the *t*-butyl protons are likely to experience rapid environmental averaging as a result of the relatively free rotation within the group. This mode of environmental averaging is less available to the aromatic protons in the naphthyl group in particular.

Molecular modelling

In the space filling MM2 Chem3D (*16*) energy minimised gas phase model structures of BNS^- complexes of the linked βCD-dimers in which the βCD annuli are constrained to an approximately common axis by the BNS^- guest, the distance from $O3^B$ to $O6^B$ in the glucopyranose unit of βCD is 780 pm. The distances measured from the mid-point of this distance projected into the centre of each of the linked annuli are 1410 pm (~30°) for 66βCD$_2$su, 1350 pm (~0°) for 36βCD$_2$su and 1240 pm (~0°) for 33βCD$_2$su, where the values in brackets are the angles between the planes of the two βCD macrocycles. These angles increase for 66βCD$_2$ur, 980 pm (~40°) and 36βCD$_2$ur, 1120 pm (~60°) seemingly because of the shortness of the urea linker and the constraining effect of the inverted $C3^A$ carbon joined to the linker (*15*). {The distance from the naphthyl C2 to the methyl substituted phenyl C4′ of BNS^- (Figure 1) is 1040 pm.} The succinamide linker is more flexible than the urea linker, and joining the linker to βCD through a primary $C6^A$ carbon appears to allow more flexibility than joining through a secondary inverted $C3^A$. These factors probably maintain the relative sizes of the interannular distances in aqueous solution, where hydrogen bonding between the βCD hydroxy groups and water occurs.

Conclusion

Generally, the fluorescence changes occurring on complexation of BNS^- are large and the K_1 values determined from them are considered more reliable than those determined from the smaller changes in UV–vis absorbance. The variations of the magnitude of K_1 (Table 1) with βCD and the linked βCD-dimers are similar for both sets of K_1. However, the K_1 determined from fluorescence changes are those discussed below. Similarly, the K_2 values derived using the fluorimetrically determined K_1 and ^{1}H NMR determined K_d as fixed values are considered the more reliable and are those discussed below.

It is seen from the variation of the magnitude of K_1 (Table 1) that the 33βCD$_2$su.BNS^- and 66βCD$_2$ur.BNS^- complexes encompass the range of stabilities of the linked βCD-dimer complexes and are 2.4 and 93 times more stable than the βCD.BNS^- complex, respectively. Generally, the increase in BNS^- complex stability with identity of the linked βCD-dimer occurs in the sequence: 33βCD$_2$su (1240 pm, 0°) < 36βCD$_2$ur (1120 pm, 60°) < 36βCD$_2$su (1350 pm, 0°) < 66βCD$_2$su (1410 pm, 30°) < 66βCD$_2$ur (980 pm, 40°), where the quantities in brackets are the interannular distances and the angles between the planes of the linked βCD annuli derived from molecular modelling. This variation is consistent with $C6^A$–$C6^A$ linking of βCD optimising K_1, while the altrose inversions in the $C3^A$–$C3^A$ and $C3^A$–$C6^A$ linked βCD annuli decrease K_1. Consequently, K_1 for 33βCD$_2$su.BNS^- and 36βCD$_2$ur.BNS^- are increased in magnitude over those for βCD.BNS^- by the approximate statistical expectation. The 22- to 93-fold increase in K_1 observed for the 66βCD$_2$su.BNS^-, 36βCD$_2$su.BNS^- and 66βCD$_2$ur.BNS^- complexes by comparison with K_1 for βCD.BNS^- indicates cooperativity in complexation of BNS^- in their linked βCD annuli. There is no obvious relationship between the interannular distances between the linked βCD and the magnitude of K_1. This is shown by K_1 increasing in the sequence 33βCD$_2$su.BNS^- < 36βCD$_2$su.BNS^- < 66βCD$_2$su.BNS^- as interannular distances decrease while K_1 increases 36βCD$_2$ur.BNS^- > 66βCD$_2$ur.BNS^- as the interannular distance decreases. This suggests that the angles between the planes of the linked βCD-dimer annuli combined with interannular distance and the presence or absence of an altrose inversion dominate the relative K_1 magnitudes.

The magnitudes of K_2 vary 79-fold for the $(BNS^-)_2$ complexes (Table 1). Generally, the increase in $(BNS^-)_2$ complex stability with identity of the host occurs in the sequence: βCD < 33βCD$_2$su < 36βCD$_2$ur < 36βCD$_2$su < 66βCD$_2$ur < 66βCD$_2$su. The ratio $K_2/K_1 = K_2'\{=$ [66βCD$_2$su.$(BNS^-)_2$]/([66βCD$_2$su.BNS^-][BNS^-]) and analogous concentrations for the other systems compares with $K_d = [(BNS^-)_2]/[BNS^-]^2 = 263\ dm^3\ mol^{-1}$ for the formation of $(BNS^-)_2$ in the absence of a host species. The variation of K_2' from 0.65 to 0.98 times the magnitude of K_d with the nature of host (Table 1) shows that the interactions of the precursor βCD.BNS^- and linked βCD-dimer.BNS^- with a second BNS^- are only slightly dependent on the host complex and have only a small effect on the formation of the successor $(BNS^-)_2$ complexes. Thus, the variation of the magnitude of $K_2 = K_1K_2'$ is dominantly determined by the magnitude of K_1.

The K_1 for complexation of TNS^- by βCD[15] (Table 1) are an order of magnitude less than those for BNS^-, and K_1 for complexation of TNS^- by the linked βCD-dimers are one to two orders of magnitude less than those for BNS^-. The K_1 variation over the five linked βCD-dimer BNS^- complexes is 39.5, while the analogous value for TNS^- is 4.37. As the only structural difference between TNS^- and BNS^- is the substitution of a methyl group by a *t*-butyl group, it is likely that the increased hydrophobicity and size of the latter are the major causes

of greater stability of the BNS^- complexes (*21*). This is probably also the cause of the formation of $\beta CD_2.TNS^-$, whereas the analogous $\beta CD_2.BNS^-$ and are not detected. Evidently the *t*-butylphenyl group is sufficiently strongly complexed by βCD to inhibit the complexing of a second βCD by the naphthyl group and the formation of $\beta CD_2.BNS^-$, whereas the less strongly complexed methylphenyl group of TNS^- allows formation of $\beta CD_2.TNS^-$.

Experimental section

Instrumental

UV–vis spectra were recorded at 0.25 nm intervals using a Cary 5000 UV–vis spectro-photometer in matched 1 cm path length quartz cells. Spectra were run against reference solutions containing identical concentrations of either βCD or the appropriate linked βCD-dimer as that in the BNS^- solutions. Fluorescence spectra were recorded at 0.5 nm intervals using a Cary Eclipse fluorimeter. Samples were thermostated at 298.2 ± 0.02 K. Solutions were prepared in phosphate buffer at pH 7.0 and $I = 0.10\ mol\ dm^{-3}$ in both studies. The ^1H 1D NMR spectra of D_2O solutions buffered at *p*D 7.0 (phosphate buffer, $I = 0.10\ mol\ dm^{-3}$, 298.2 K) were run in 5 mm NMR tubes thermostated at 298.2 ± 0.1 K on a Varian Gemini ACP-300 MHz NMR spectrometer operating at 300.145 MHz. The ^1H 2D ROESY NMR spectra were run on a Varian Inova 600 NMR spectrometer operating at 599.957 MHz with a delay time of 300 ms. Chemical shifts were measured from external trimethylsilyl-propiosulphonic acid in D_2O.

Materials

Phosphate buffer was prepared from analytical grade Na_2HPO_4 (BDH) and KH_2PO_4 (Ajax) as described in the literature (*22*). β-Cyclodextrin was a gift from Nihon Shokuhin Kako Co. and was used without further purification. All other reagents were of good quality reagent grade. Sodium 6-(4′-*t*-butylphenylamino)-naphthalene-2-sulphonate, NaBNS, was prepared as described in the literature and gave a good elemental analysis and gave UV–vis and ^1H 1D NMR spectra identical to those reported (*23*). The linked βCD-dimers *N*,*N*′-bis(3^A-deoxy-3^A-β-cyclodextrin)-succinamide (33βCD_2su), *N*-(3^A-deoxy-3^A-β-cyclodextrin)-*N*′-(6^A-deoxy-6^A-β-cyclodextrin)-succinamide (36βCD_2su), and *N*,*N*′-bis(6^A-deoxy-6^A-β-cyclodextrin)-succinamide (66βCD_2su), *N*-(3^A-deoxy-3^A-β-cyclodextrin)-*N*′-(6^A-deoxy-6^A-β-cyclo-dextrin)urea (36βCD_2ur) and *N*,*N*′-bis(6^A-deoxy-6^A-β-cyclodextrin)urea (66βCD_2ur) were prepared as in the literature and elemental analyses and ^1H and ^{13}C ^1D NMR spectra were in good agreement with those reported (*7, 15*).

Data analysis

The appropriate algorithms were iteratively fitted to experimental δ data to determine K_d, K_1 and K_2 using the in-house program Specfit (*24*) for the UV–vis and fluorimetric data and the HypNmr 2003 commercial program for the ^1H 1D NMR δ data (*25*).

Molecular modelling

Molecular modelling and energy minimisations were performed using Chem3D Ultra 8.0 (*16*).

Electronic supplementary information available

All UV–vis, fluorescence and ^1H NMR spectra and associated data fits mentioned in the text but not shown in Figures S1–S27.

Acknowledgements

The award of a MOET scholarship by the Vietnamese Government to Duc-Truc Pham, and the support of this study by the Australian Research Council and the University of Adelaide and a gift of β-cyclodextrin from Nihon Shokuhin Kako Co., Japan are gratefully acknowledged.

References

(1) Szejtli, J. *Chem. Rev.* **1998**, *98*, 1743–1754; Gattuso, G.; Nepogodiev, S.A.; Stoddart, J.F. *Chem. Rev.* **1998,** *98*, 1959–1976; Easton, C.J.; Lincoln, S.F. In *Modified Cyclodextrins: Scaffolds and Templates for Supramolecular Chemistry*; Imperial College Press: London, 1999; Wenz, G.; Han, B.-H.; Muller, A. *Chem. Rev.* **2006**, *106*, 782–817.
(2) Harada, A. *Acc. Chem. Res.* **2001**, *34*, 456–461.
(3) Lock, J.S.; May, B.L.; Clements, P.; Lincoln, S.F.; Easton, C.J. *Org. Biomol. Chem.* **2004**, *2*, 1381–1386; Lock, J.S.; May, B.L.; Clements, P.; Lincoln, S.F.; Easton, C.J. *J. Incln. Phenom. Macrocycl. Chem.* **2004**, *50*, 13–18.
(4) Liu, Y.; Chen, Y. *Acc. Chem. Res.* **2006**, *39*, 681–691.
(5) Chiu, S.-H.; Myles, D.C.; Garrell, R.L.; Stoddart, J.F. *J. Org. Chem.* **2000**, *65*, 2792–2796.
(6) Coates, J.H.; Easton, C.J.; van Eyk, S.J.; Lincoln, S.F.; May, B.L.; Walland, C.B.; Williams, M.L. *J. Chem. Soc., Perkins Trans. 1* **1990**, 2619–2620.
(7) Easton, C.J.; van Eyk, S.J.; Lincoln, S.F.; May, B.L.; Papageorgiou, J.; Williams, M.L. *Aust. J. Chem.* **1997**, *50*, 9–14.
(8) Haskard, C.A.; Easton, C.J.; May, B.L.; Lincoln, S.F. *J. Phys. Chem.* **1996**, *100*, 14457–14461.
(9) Haskard, C.A.; May, B.L.; Kurucsev, T.; Lincoln, S.F.; Easton, C.J. *J. Chem. Soc. Faraday Trans.* **1997**, *93*, 279–282; Cieslinski, M.M.; Clements, P.; May, B.L.; Easton, C.J.; Lincoln, S.F. *J. Chem. Soc., Perkin Trans. 2* **2002**, 947–952.
(10) Breslow, R.; Greenspoon, N.; Guo, T.; Zarzycki, R. *J. Am. Chem. Soc.* **1989**, *111*, 8296–8297.
(11) Zhang, B.; Breslow, R. *J. Am. Chem. Soc.* **1997**, *119*, 1676–1681; Breslow, R.; Dong, S.D. *Chem. Rev.* **1998**, *98*,

1997–2011; Breslow, R.; Belvedere, S.; Gershell, L.; Leung, D. *Pure Appl. Chem.* **2000**, *72*, 333–342.
(12) Liu, Y.; Li, B.; You, C.-C.; Wada, T.; Inoue, Y. *J. Org. Chem.* **2001**, *66*, 225–232.
(13) Liu, Y.; Yang, Y.-W.; Yang, E.-C.; Guan, X.-D. *J. Org. Chem.* **2004**, *69*, 6590–6602.
(14) West, L.C.; Wyness, O.; May, B.L.; Clements, P.; Lincoln, S.F.; Easton, C.J. *Org. Biomol. Chem.* **2003**, *1*, 887–894; Wyness, O.; May, B.L.; Clements, P.; Lincoln, S.F.; Easton, C.J. *Aust. J. Chem.* **2004**, *57*, 571–576.
(15) Pham, D.-T.; Clements, P.; Easton, C.J.; Papageorgiou, J.; May, B.L.; Lincoln, S.F. *N. J. Chem.* **2008**, *32*, 712–718.
(16) Chem3D Ultra. CambridgeSoft Co., 100 Cambridge Park Drive, Cambridge, MA 02140, USA.
(17) Clarke, R.J.; Coates, J.H.; Lincoln, S.F. *J. Chem. Soc. Faraday Trans. I* **1984**, *80*, 3119–3133; Schiller, R.L.; Coates, J.H.; Lincoln, S.F. *J. Chem. Soc. Faraday Trans. I* **1984**, *80*, 1257–1266; Schiller, R.L.; Lincoln, S.F.; Coates, J.H. *J. Chem. Soc. Faraday Trans. I* **1986**, *82*, 2123–2132; Clarke, R.J.; Coates, J.H.; Lincoln, S.F. *J. Chem. Soc. Faraday Trans. I* **1986**, *82*, 2333–2343. (In these references 'annular radius' should read 'annular diameter'.)
(18) Karukstis, K.K.; Krekel, D.A.; Weinberger, D.A.; Bittker, R.A.; Naito, N.R.; Bloch, S.H. *J. Phys. Chem.* **1995**, *99*, 449–451.
(19) Hicks, J.; Vandersall, M.; Babarogic, Z.; Eisenthal, K.B. *Chem. Phys. Lett.* **1985**, *116*, 18–24.
(20) Schneider, H.-J.; Hacket, F.; Rüdiger, V.; Ikeda, H. *Chem. Rev.* **1998**, *98*, 1755–1785.
(21) Höfler, T.; Wenz, G. *J. Incl. Phenom. Mol. Recogn. Chem.* **1996**, *25*, 81–84.
(22) King, E.J.; Sperry, W.M. *Biochemists' Handbook*; Spon: London, 1971.
(23) Kosower, E.M.; Dodiuk, H.; Tanizawa, K.; Ottolenghi, M.; Orbach, N. *J. Am. Chem. Soc.* **1975**, *97*, 2167–2178.
(24) Kurusev, T. University of Adelaide, 1984.
(25) Frassineti, C.; Ghelli, S.; Gans, P.; Sabatini, A.; Moruzzi, M.S.; Vacca, A. *Anal. Biochem.* **1995**, *231*, 374–382. HypNmr 2003, Protonic Software, 2, Templegate Avenue, Leeds LS15 0HD, UK.